Ultrasound-based sensors for respiratory motion assessment in multimodality PET imaging

Document license:
TAVERNE

DOI:
10.1088/1361-6560/ac4213

Document status and date:
Published: 19/01/2022

Document Version:
Publisher's PDF, also known as Version of Record (includes final page, issue and volume numbers)

Please check the document version of this publication:

• A submitted manuscript is the version of the article upon submission and before peer-review. There can be important differences between the submitted version and the official published version of record. People interested in the research are advised to contact the author for the final version of the publication, or visit the DOI to the publisher's website.
• The final author version and the galley proof are versions of the publication after peer review.
• The final published version features the final layout of the paper including the volume, issue and page numbers.

Link to publication

Download date: 16. Nov. 2023

IPEM
Institute of Physics and
Engineering in Medicine

NOTE

Ultrasound-based sensors for respiratory motion assessment in multimodality PET imaging

View the article online for updates and enhancements.
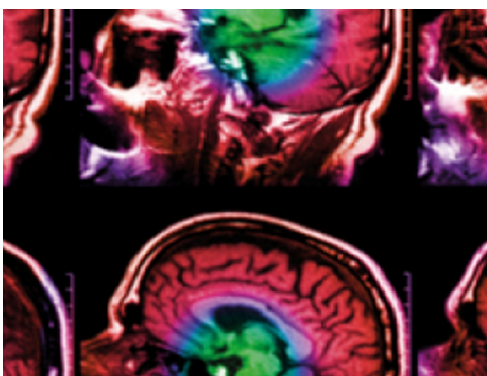
IPEM | IOP

Series in Physics and Engineering in Medicine and Biology

Your publishing choice in medical physics, biomedical engineering and related subjects.

Start exploring the collection—download the first chapter of every title for free.

Physics in Medicine & Biology

IPEM Institute of Physics and Engineering in Medicine

NOTE

Ultrasound-based sensors for respiratory motion assessment in multimodality PET imaging

Bruno Madore[1,8] , Gabriela Belsley[2,8] , Cheng-Chieh Cheng[3] , Frank Preiswerk[4], Marie Foley Kijewski[1], Pei-Hsin Wu[5] , Laurel B Martell[1], Josien P W Pluim[6], Marcelo Di Carli[1] and Stephen C Moore[7]

[1] Department of Radiology, Brigham and Women's Hospital, Harvard Medical School, Boston, MA 02115, United States of America
[2] Oxford Centre for Clinical Magnetic Resonance Research, Radcliffe Department of Medicine, University of Oxford, Oxford, United Kingdom
[3] Department of Computer Science and Engineering, National Sun Yat-sen University, Kaohsiung, Taiwan
[4] Amazon Robotics, Westborough, MA, United States of America
[5] Department of Electrical Engineering, National Sun Yat-sen University, Kaohsiung, Taiwan
[6] Department of Biomedical Engineering, Eindhoven University of Technology, The Netherlands
[7] Department of Radiology, University of Pennsylvania Perelman School of Medicine, Philadelphia, PA 19104, United States of America
[8] The first two authors contributed equally to this work.

E-mail: bruno@bwh.harvard.edu

Abstract

Breathing motion can displace internal organs by up to several cm; as such, it is a primary factor limiting image quality in medical imaging. Motion can also complicate matters when trying to fuse images from different modalities, acquired at different locations and/or on different days. Currently available devices for monitoring breathing motion often do so indirectly, by detecting changes in the outline of the torso rather than the internal motion itself, and these devices are often fixed to floors, ceilings or walls, and thus cannot accompany patients from one location to another. We have developed small ultrasound-based sensors, referred to as 'organ configuration motion' (OCM) sensors, that attach to the skin and provide rich motion-sensitive information. In the present work we tested the ability of OCM sensors to enable respiratory gating during *in vivo* PET imaging. A motion phantom involving an FDG solution was assembled, and two cancer patients scheduled for a clinical PET/CT exam were recruited for this study. OCM signals were used to help reconstruct phantom and *in vivo* data into time series of motion-resolved images. As expected, the motion-resolved images captured the underlying motion. In Patient #1, a single large lesion proved to be mostly stationary through the breathing cycle. However, in Patient #2, several small lesions were mobile during breathing, and our proposed new approach captured their breathing-related displacements. In summary, a relatively inexpensive hardware solution was developed here for respiration monitoring. Because the proposed sensors attach to the skin, as opposed to walls or ceilings, they can accompany patients from one procedure to the next, potentially allowing data gathered in different places and at different times to be combined and compared in ways that account for breathing motion.

Introduction

Positron emission tomography (PET) allows positron-emitting radiotracers, based on radionuclides such as ^{18}F, ^{11}C, ^{13}N or ^{15}O, to be detected in concentrations as low as the picomolar range (Pichler *et al* 2008). Consequently, for many types of cancer, PET has unequaled sensitivity for detecting tumors and metastases (Beyer *et al* 2003). Complementary imaging from CT or MRI is needed for attenuation correction and determination of the anatomic location of any suspected disease seen in the PET images. With either MRI or CT (Sawicki *et al* 2016a, 2016b, Raad *et al* 2016, Chandarana *et al* 2013, Riola-Parada *et al* 2016, Dawood *et al* 2007, 2006), PET is the gold standard for cancer assessment and tumor staging. However, because PET
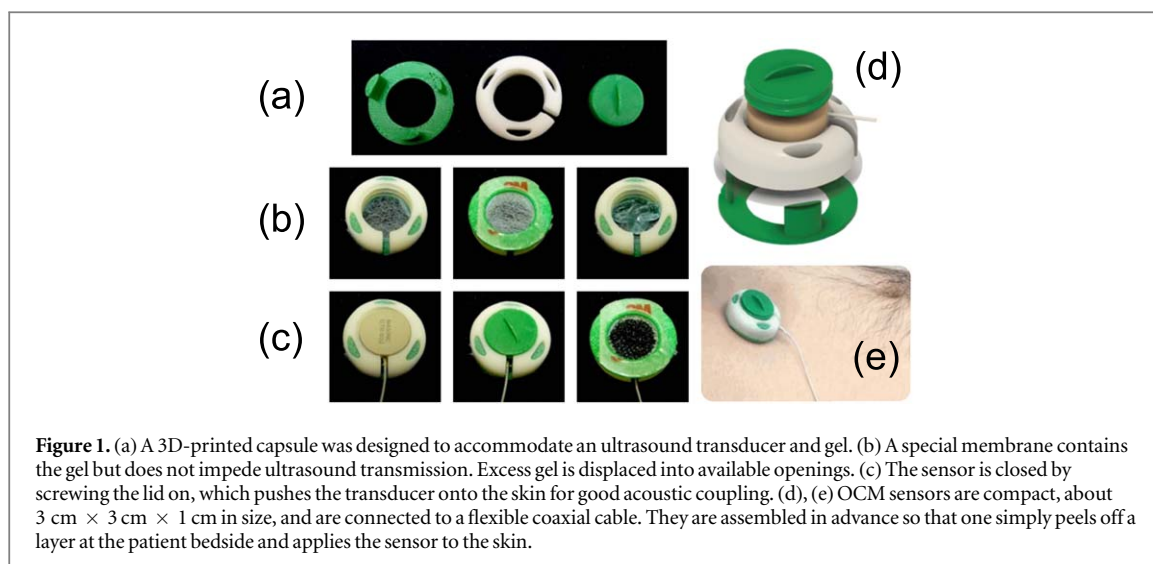
Figure 1. (a) A 3D-printed capsule was designed to accommodate an ultrasound transducer and gel. (b) A special membrane contains the gel but does not impede ultrasound transmission. Excess gel is displaced into available openings. (c) The sensor is closed by screwing the lid on, which pushes the transducer onto the skin for good acoustic coupling. (d), (e) OCM sensors are compact, about 3 cm × 3 cm × 1 cm in size, and are connected to a flexible coaxial cable. They are assembled in advance so that one simply peels off a layer at the patient bedside and applies the sensor to the skin.

acquisitions may last several minutes or longer, breathing motion can be problematic (Calabrese *et al* 1998, McClelland *et al* 2013, Dasari *et al* 2014a, 2014b) as it causes image blurring and respiratory artifacts. In turn, degradations in image quality (Osman *et al* 2003, Erdi *et al* 2004, Keller *et al* 2013) may impact treatment planning (Nehmeh *et al* 2004, Osman *et al* 2003) and complicate the fusion of multi-modality images. Multi-modality fusion requires a motion management system compatible with many different systems.

One simple approach to minimize motion is based on deep-inspiration breath-holding, but this requires a level of cooperation and repeatability that often cannot be attained by oncology patients and, furthermore, cannot be maintained for the typical PET acquisition time. Respiratory bellows (Hope *et al* 2015), spirometers (Zhang *et al* 2003), radar-like technology (Pfanner *et al* 2013) and optical trackers (Nehmeh *et al* 2002, Nehmeh *et al* 2004, O'Connor *et al* 2013, Nehmeh and Erdi 2008, Boucher *et al* 2004, Dawood *et al* 2007, 2006) can be used to monitor breathing motion. Bellows and optical trackers detect only changes that occur on the outline of the torso, and the link between such changes and actual internal motion can be complex (Koch *et al* 2004, Chi *et al* 2006, Fayad *et al* 2012, Dasari *et al* 2014a, 2014b, Ruan *et al* 2008, Dasari *et al* 2017). Bellows and spirometers model respiration as a one-dimensional problem, which oversimplifies the nature of human breathing (Madore *et al* 2021). Ultrasound scanners can also be used to track internal motion, as tested in an MRI environment (Günther and Feinberg 2004, Petrusca *et al* 2013, Kording *et al* 2015); however, long cables and difficulties positioning the ultrasound probe on the patient's body inside the bore of a scanner can increase the complexity of the clinical workflow. Alternatively, self-gating or 'data-driven' approaches based on tracking changes in the PET counts over time within a given region of interest are available (Kesner *et al* 2014, Ren *et al* 2017, Schleyer *et al* 2011, Hess *et al* 2017, Schleyer *et al* 2014, Liu *et al* 2011). However, data-driven PET methods function only when the patient happens to lie within a PET scanner and would not be relevant for multi-modality purposes. In other words, self-gating abilities are attached to the PET scanner itself, and as such cannot accompany a patient through procedures at different locations.

We developed small ultrasound (US)-based sensors along with algorithms to interpret their signals (Preiswerk *et al* 2018, Cheng *et al* 2018, Madore *et al* 2021). We named these devices 'organ configuration motion' (OCM) sensors because they generate signals that are sensitive to the 'configuration' of internal organs at any given moment; furthermore, such configurations are dynamic in nature due to the underlying organ motion. In contrast to other devices mentioned above, OCM sensors attach to the skin and can accompany patients through sequential procedures. The emitted and reflected US waves probe the body to sense internal organ motion directly, rather than indirectly through changes in external body surfaces, contours, or projected count density. High dimensionality is a further advantage of OCM signals; at each time point, an OCM trace may consist of up to 20 000 samples (Preiswerk *et al* 2017, Cheng *et al* 2018, Preiswerk *et al* 2015, Preiswerk *et al* 2018), compared to 1 value for bellows, and roughly a dozen for optical tracking (*x*, *y* and *z* coordinates for a few reflective markers). OCM sensors are small, about 3 cm × 3 cm × 1 cm in size (see figure 1), and relatively inexpensive. To place an OCM sensor on a patient one simply peels off a protective layer and applies the adhesive surface to the skin. OCM sensors could, in principle, be placed on the skin for a first imaging session (e.g. a PET/CT exam); the position could be marked on the skin with ink, and the sensors could be re-installed as closely as possible to the original location on a different day for a second imaging session (e.g. an MRI exam) or treatment (e.g. radiation therapy). OCM sensors were developed with multi-modality imaging in mind and have already

been tested in MRI (Preiswerk *et al* 2015, Madore *et al* 2021). While our recent work (Madore *et al* 2021) focused on developing algorithms to better interpret the OCM signals, the present work extends the sensor applications from an MRI to a PET environment. More specifically, the synchronization of OCM and PET data streams and the reconstruction of images from combined OCM and PET information were the main technical challenges tackled here.

The OCM + PET approach proposed here can, in principle, reduce blurring artifacts in abdominal and thoracic PET images acquired in the presence of breathing motion. However, the availability of alternative motion-compensation approaches, such as data-driven methods as described above, may tend to reduce the clinical need for OCM sensors for this purpose. In our view at least, the proposed approach may eventually prove most helpful in the context of separate imaging session, for example an OCM + MRI and an OCM + PET session, with OCM signals acting as a bridge between the two to facilitate image fusion. However, such more elaborate applications should be considered as future work, and the present work focuses on the OCM + PET aspect only.

Materials and methods

OCM setup

The OCM sensors included a 1 MHz MRI-compatible single-element US transducer (Imasonic, Voray-sur-l'Ognon, France), see figure 1. During PET imaging, an OCM sensor was 'fired' 100 times per second, and after each firing useful signals were received for about 0.2 ms, i.e. about 30 cm of travel at 1540 m s^{-1} (~15 cm of depth). Each firing involved a short negative voltage pulse that approximated a delta function, about 0.5 μs in duration and about -200 V in size, being applied to the transducer. An Olympus 5072PR pulser-receiver was used to fire the sensor, and a PCI digitizer card NI 5122 mounted into a desktop PC was used to digitize the returning US signals.

As usual with US devices, the voltage was relatively high but the current (and hence power), as well as risk, were low. The 'spatial peak temporal average' (SPTA) intensity provided by the vendor was $I_{SPTA} = 51.5\ \mu$W cm^{-2}, far below the FDA limit of 720 mW cm^{-2} for non-ophthalmic applications. Through hydrophone tests we evaluated the mechanical index (MI) at 1.06×10^{-3}, much below the FDA limit of 1.9. The small area of the transducer and the diverging nature of the field it creates help explain these small I_{SPTA} and MI values.

Timestamps and synchronization

Strategies were needed to synchronize the simultaneous data streams (O'Connor *et al* 2013) from PET and OCM hardware, so that PET coincidence events and OCM signals could be placed on a common time axis. To do this, synchronization triggers were digitally created and applied simultaneously to both streams. More specifically, a USB port of the PC also equipped with the digitizer card (subsection 'OCM setup' above) was connected to the respiratory gating port of the PET/CT scanner through modified cables/connectors. At irregular time intervals, incoming OCM traces were flagged at the same time as voltages were placed on given pins of the USB port. These voltage pulses, applied to the PET/CT respiratory trigger port, led to time-stamped entries being created in the PET/CT raw data (list-mode) file. As a result, a non-periodic pattern of time tags appeared in both OCM and PET raw data files, allowing OCM and PET data to be synchronized without ambiguity. These tags occurred on average every 3 s, but a modulation on the tag-to-tag interval, ΔT_n, ensured that the overall pattern would be non-periodic and thus allow an unequivocal match between the OCM traces and the PET timestamps:

$$\Delta T_n = n\theta - floor(n\theta) - 1/2; \ \theta = 1 - 1/\phi, \tag{1}$$

where n is an integer that counts tags, and ϕ is the golden ratio, $(1 + \sqrt{5})/2$. The right-hand side of equation (1), $n\theta - floor(n\theta) - 1/2$, is contained in the $[-0.5, 0.5]$ interval, appears pseudo-random as a function of n, and has a mean value of zero. As a result, adding ΔT_n to the tag-to-tag interval does not change its mean value, which remains 3 s, but it makes the interval vary from one tag to the next in pseudo-random fashion in the interval from 2.5 to 3.5 s, thus removing any time-shift ambiguity that a constant interval would have caused.

Phantom experiments

Using a Siemens Biograph mCT scanner, PET/CT images of a phantom were obtained with and without an OCM sensor in the FOV, to test for presence of artifacts. OCM sensors are not meant to 'image', so they do not need to be oriented or lined up with any particular organ of interest, as they are simply meant here to generate motion-sensitive signals that can be employed for gating purposes. Because the sensor does not need to be placed near suspected lesions, there would be no compelling reason to place it within the PET/CT imaging FOV, but if

it were by mistake included in the FOV one would like to know whether this could deleteriously affect the PET and/or CT image quality.

In a second phantom-based test, a motion phantom was constructed by placing a ^{18}F-fluorodeoxyglucose (FDG) solution into a conical centrifuge tube, and then fixing this tube to a small moveable plane. The tube and plane were placed in a water-containing bath along with a submerged OCM sensor. While the plane and tube were manually moved vertically up and down, the tube's contents were imaged by a GE DRX/VCT PET/CT scanner, and the OCM sensor captured the ongoing motion.

In vivo scans

Two patients scheduled for an oncologic PET/CT exam were scanned for an additional 10 min single-station PET scan, with OCM sensor in place. The project was approved by the IRB committee at our institution (protocol number 2002P001824), the research was conducted in accordance with the principles embodied in the Declaration of Helsinki and in accordance with local statutory requirements, and all participants gave written informed consent to participate in the study. These *in vivo* scans involved the same GE DRX/VCT PET/CT scanner as mentioned above for the motion phantom scan. The research PET scan was performed immediately after the clinical one, using the same CT data, so that no additional tracer was injected and no extra CT scan was performed. Accordingly, the radiation dose was not increased for participating patients beyond the dose of the clinical exam they were prescribed.
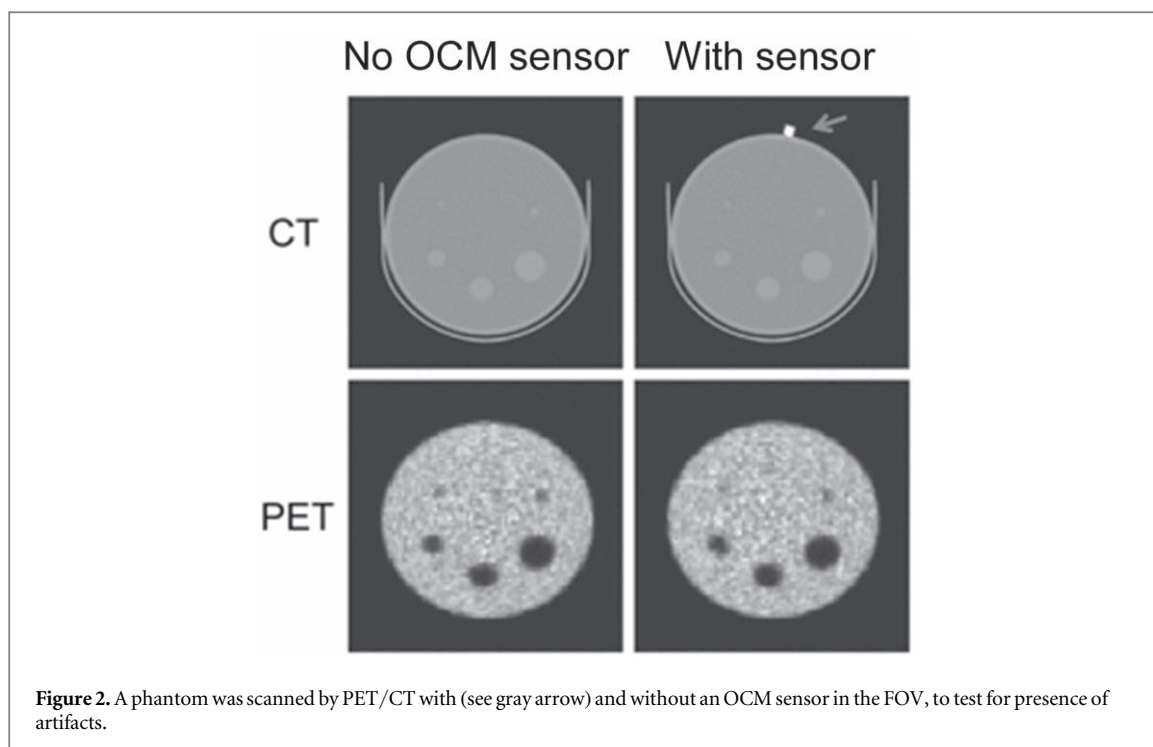
An OCM sensor was fixed to the abdomen, a few cm below the ribs and to the right of the midline. In general, placing the sensor anywhere on the thorax should provide the type of breathing-dependent signals needed for respiratory gating, but placing sensors over the liver (i.e. just below the ribs and on the right side), as done here, tended to avoid any strong reflections from any possible shallow tissue/bone or tissue/air interfaces, allowing ultrasound waves to penetrate and sample tissues deeper within the abdominal cavity. OCM signals (0.2 ms per trace, 100 traces per s) were acquired throughout the 10 min research PET scan. In terms of workflow, 4 min were needed to set up the sensor and associated hardware between the end of the clinical scan and the beginning of the research scan, and 1 min was needed afterward to remove all equipment from the clinical suite upon completion of the research scan.

OCM signal processing

As demonstrated in our prior work (Preiswerk *et al* 2015, Cheng *et al* 2018, Preiswerk *et al* 2017, Preiswerk *et al* 2018), OCM signals are very sensitive to internal motion, and several different algorithms have been tested to extract such information from the raw signals. Some algorithms based on machine learning were more involved and expressed the motion information in more elaborate fashion as projections onto manifolds in function space (Preiswerk *et al* 2018), while others generated more intuitive breathing waveforms based primarily on the phase of the US signals (Madore *et al* 2021), and others generated breathing waveforms primarily based on the magnitude of envelope-detected US signals (Cheng *et al* 2018). In the present feasibility test the simpler, latter approach was implemented. The envelope of the raw ultrasound signal was extracted using a Hilbert Transform. As the breathing cycle progressed from inhalation to exhalation (and vice versa), the distance between sensor and echogenic tissues increased and decreased, leading to time shifts in the received signals. By selecting a depth range so that only similarly moving tissues are considered, cross correlations were performed between a reference trace and all other OCM traces in turn, to evaluate the time shift and the associated breathing-related changes in sensor-to-tissue distances. Breathing-related variations in time shift and distance readily allowed expiration periods to be detected, and phase-based respiratory gating (Abdelnour *et al* 2007, Dawood *et al* 2007, 2006, Lu *et al* 2006) to be performed. Each breathing period was associated with a phase ranging from 0 to 2π, and N respiratory gates were created by generating N bins each one $2\pi/N$ wide. The value of N, which represents a tradeoff between temporal resolution and SNR, was set here within the range of 8–10 respiratory frames.

Image reconstruction

Detector-coincidence records from the PET raw data (i.e. list-mode) file were read and sorted according to the respiratory state as determined by time-matched OCM signals. Eight to ten (smaller) list-mode files, one per respiratory state, were created with custom-built Matlab software and then reconstructed with scanner software, with all usual corrections performed. The reconstructed volumetric field-of-view (FOV) consisted of 47 axial slices covering a 15.4 cm range in the superior/inferior direction, with a 60 cm circular FOV in the axial plane. The reconstruction settings were 3D whole body, 21 subsets and 2 iterations using a standard z axis filter and a post-processing smoothing filter with 5.14 mm full width at half maximum. A CT-based attenuation correction with no contrast correction or shift, but corrected by singles, dead time and scatter was applied. Averaging

Figure 2. A phantom was scanned by PET/CT with (see gray arrow) and without an OCM sensor in the FOV, to test for presence of artifacts.

images over all breathing states yielded images that were, for all intents and purposes, identical to those reconstructed by the clinical scanner at the time of the exam.

Results

Phantom results

OCM sensors should be placed so that they are not included in the imaged FOV. They are not meant to image the anatomy of interest, but rather to gather motion-sensitive signals, and as such there is no reason to place them in the FOV. Even so, their effect on CT and PET imaging was tested: as seen in figure 2, it is possible to build OCM sensors that create no visible artifact in either CT or PET. A second sensor was tested under CT which did produce visible streaking artifacts (data not shown), the main difference between the two is believed to be the amount and/or type of solder used. At any rate, there seems to be no clear rationale for placing sensors within the imaged FOV and as such they should be placed well out of it.

A moving phantom was imaged using a simultaneous PET and OCM acquisition while undergoing a mostly vertical, up-and-down, pseudo-periodic motion. The raw PET list-mode data were sorted according to the motion information captured by the OCM signals, and each temporal phase bin was individually reconstructed. As shown in figure 3, using OCM signals to characterize displacements, PET images were created that successfully captured the phantom at different locations along its range of motion.

In vivo results

Detector-coincidence data in the PET list-mode file were read and sorted according to the respiratory state as determined by OCM (see figure 4). Eight different 3D respiratory gates were reconstructed and breathing motion could be visualized by displaying these gates in a movie loop. Patient #1 had a large lesion with a partially necrotic central region, in the upper part of the left lung (see figures 5(a), (b)). This lesion was mostly static, so that different respiratory gates all captured the lesion in essentially the same location. Averaging all reconstructed gates (figures 5(a), (b)) led to images that were nearly identical to that generated by the scanner (the absolute difference image, amplified by 10-fold, is shown in figure 5(c)).

Patient #2 was a mesothelioma patient with several lesions; some of these lesions were attached to relatively stationary tissues and moved very little throughout the breathing cycle, while others moved by up to 10 mm or more, primarily in the superior–inferior (S/I) direction. Figure 6 shows two different coronal slices at expiration, inspiration and with all gates averaged. A maximum-intensity projection was applied in the right–left (R/L) direction, over the S/I extend indicated by dashed gray lines, leading to the plots in figures 6(b), (d).
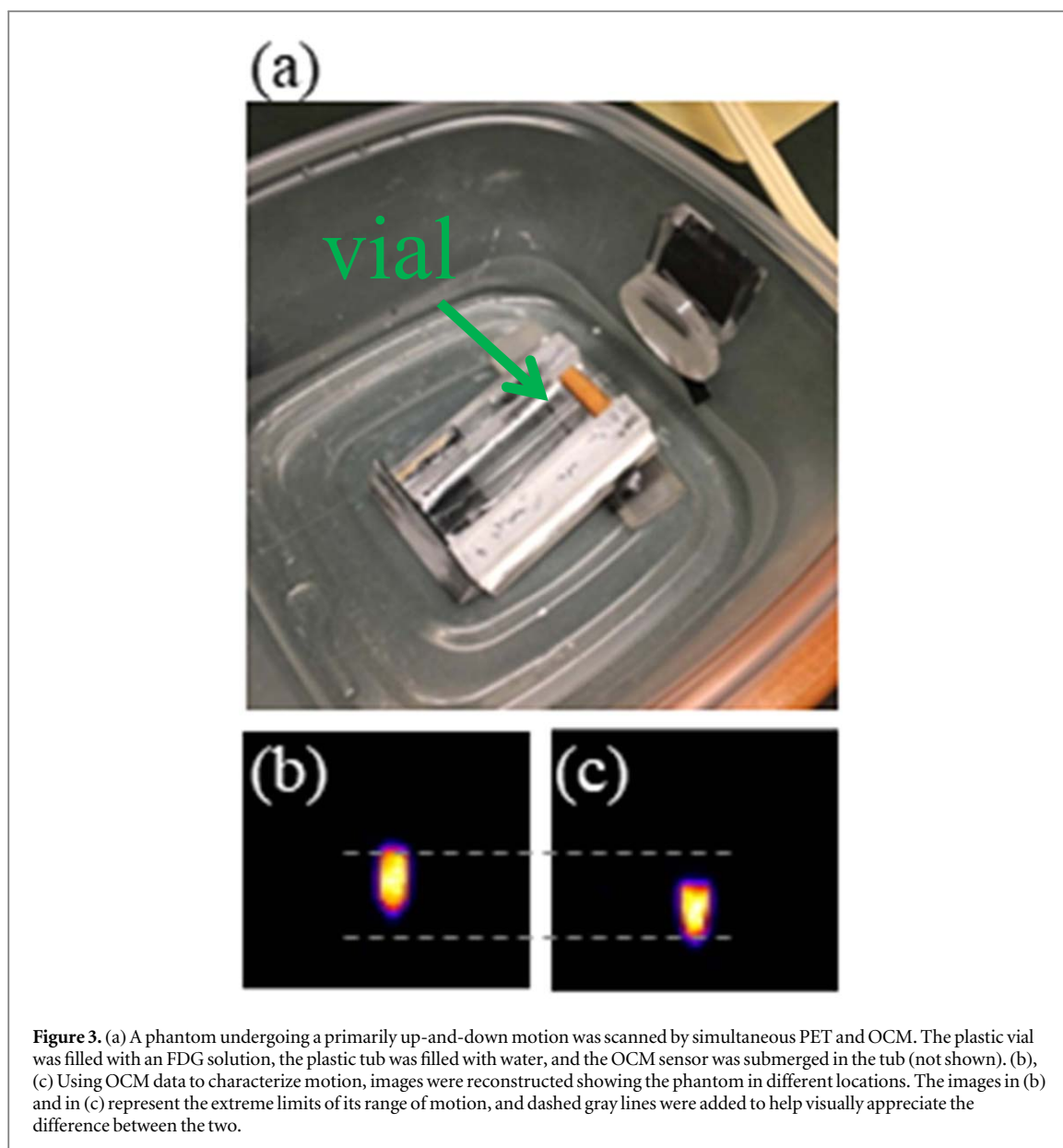
Figure 3. (a) A phantom undergoing a primarily up-and-down motion was scanned by simultaneous PET and OCM. The plastic vial was filled with an FDG solution, the plastic tub was filled with water, and the OCM sensor was submerged in the tub (not shown). (b), (c) Using OCM data to characterize motion, images were reconstructed showing the phantom in different locations. The images in (b) and in (c) represent the extreme limits of its range of motion, and dashed gray lines were added to help visually appreciate the difference between the two.

Discussion

Signals from our ultrasound-based OCM sensors were used to enable respiratory gating in a PET acquisition. Compared to alternative respiratory gating approaches, advantages of the OCM-based approach include low cost (Willey *et al* 2020), rich motion-related signals, and hardware that is attached to the patient rather than to floors, ceiling or walls. Consequently, they can accompany the patient from one location to another. While the primary purpose of this work was to adapt our sensor system to the PET environment, the rich motion information it captured was not necessarily fully exploited in the current image reconstruction software, which was based on a relatively simple form of respiratory compensation called phase-based gating. For this reason, the potential of the present hardware system for improved respiratory gating may not have been yet fully realized, and we are still developing algorithms to extract and utilize the available information more thoroughly (Madore *et al* 2021). A little like an optical camera that can focus on different depths, information about the different motion types that occur at different tissue depths (e.g. figure 4) might help inform an amplitude-based algorithm optimized for the tissue depth(s) of interest. In comparison, the current phase-based implementation can be seen as a useful first step that allowed the hardware prototype to be successfully tested.

The present technical work extended the range of applicability of OCM sensors to PET imaging, and in so doing laid the groundwork for future multi-modal applications, for example using OCM sensors as a bridge from PET to MRI or radiation therapy, i.e. to allow information obtained at one location to inform decisions
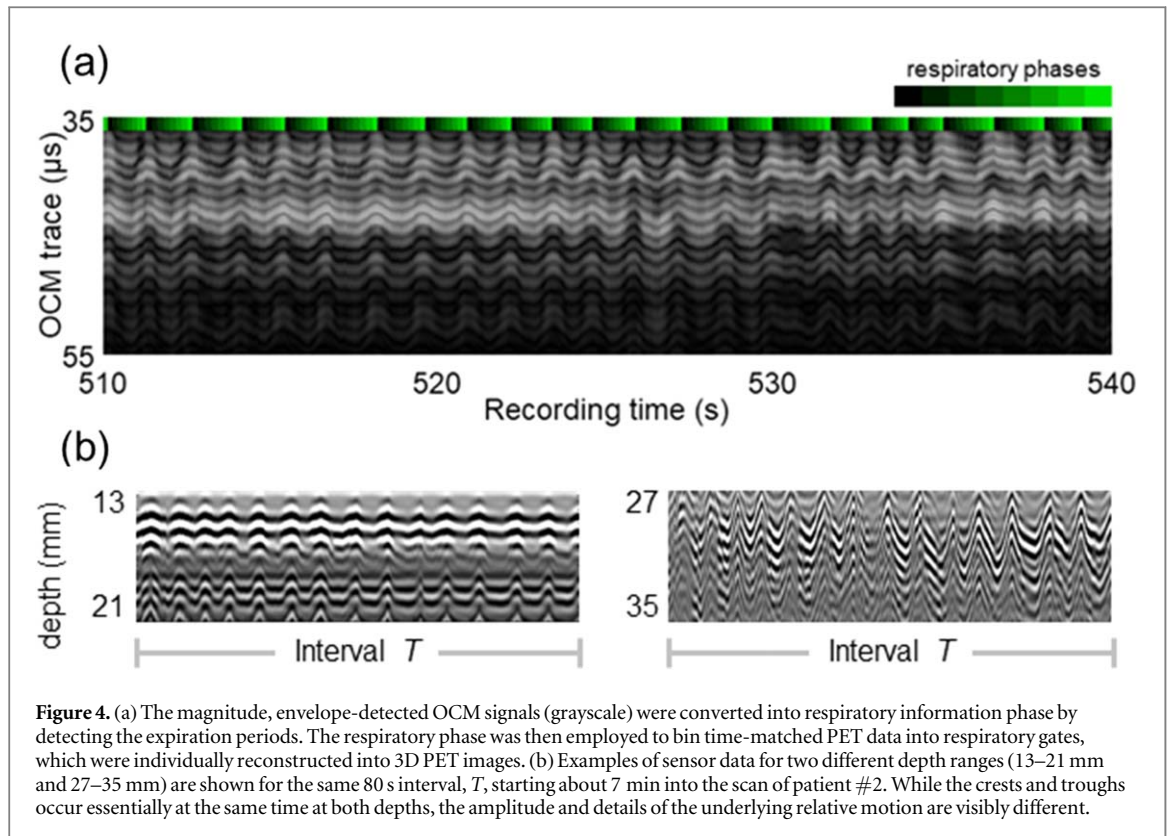
Figure 4. (a) The magnitude, envelope-detected OCM signals (grayscale) were converted into respiratory information phase by detecting the expiration periods. The respiratory phase was then employed to bin time-matched PET data into respiratory gates, which were individually reconstructed into 3D PET images. (b) Examples of sensor data for two different depth ranges (13–21 mm and 27–35 mm) are shown for the same 80 s interval, T, starting about 7 min into the scan of patient #2. While the crests and troughs occur essentially at the same time at both depths, the amplitude and details of the underlying relative motion are visibly different.
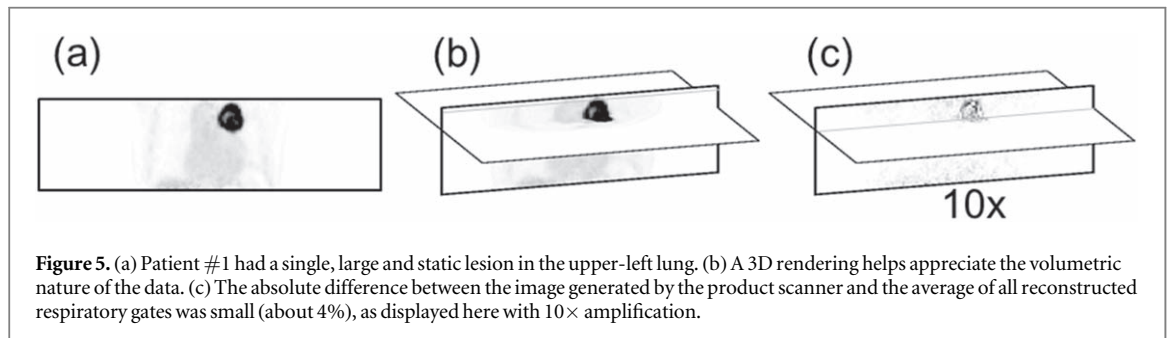

Figure 5. (a) Patient #1 had a single, large and static lesion in the upper-left lung. (b) A 3D rendering helps appreciate the volumetric nature of the data. (c) The absolute difference between the image generated by the product scanner and the average of all reconstructed respiratory gates was small (about 4%), as displayed here with 10× amplification.
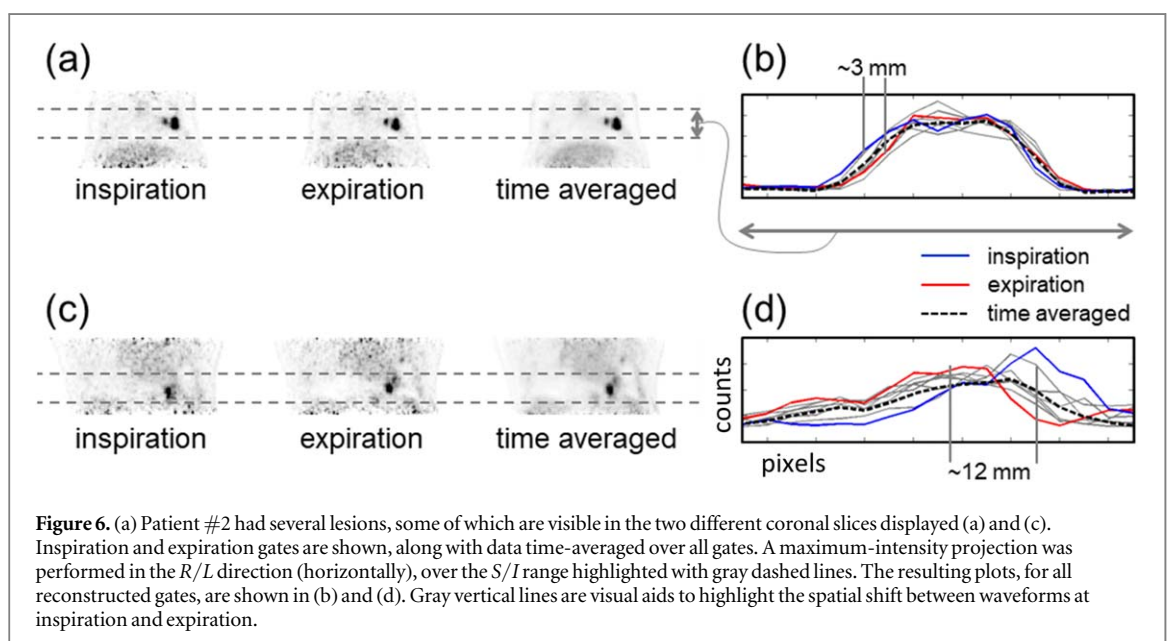

Figure 6. (a) Patient #2 had several lesions, some of which are visible in the two different coronal slices displayed (a) and (c). Inspiration and expiration gates are shown, along with data time-averaged over all gates. A maximum-intensity projection was performed in the R/L direction (horizontally), over the S/I range highlighted with gray dashed lines. The resulting plots, for all reconstructed gates, are shown in (b) and (d). Gray vertical lines are visual aids to highlight the spatial shift between waveforms at inspiration and expiration.

made at another in a manner that takes breathing motion into account. Limitations of the present work include a low number of patients.

Conclusions

A relatively inexpensive approach was presented that allows respiration monitoring in a PET environment. An important characteristic of this approach is the fact that hardware attaches to the patient rather than to floors, ceiling or walls and as such can accompany the patient from one setting to another, potentially allowing information obtained in different times and places to be combined in a manner that takes breathing into account.

Acknowledgments

ORCID iDs

Bruno Madore ⓘ https://orcid.org/0000-0002-5606-8771
Gabriela Belsley ⓘ https://orcid.org/0000-0001-5273-2340
Cheng-Chieh Cheng ⓘ https://orcid.org/0000-0001-5833-5661
Pei-Hsin Wu ⓘ https://orcid.org/0000-0001-8413-3676

References

Abdelnour A F *et al* 2007 Phase and amplitude binning for 4D-CT imaging *Phys. Med. Biol.* **52** 3515–29

Beyer T, Antoch G, Blodgett T, Freudenberg L F, Akhurst T and Mueller S 2003 Dual-modality PET/CT imaging: the effect of respiratory motion on combined image quality in clinical oncology *Eur. J. Nucl. Med. Mol. Imaging* **30** 588–96

Boucher L, Rodrigue S, Lecomte R and Benard F 2004 Respiratory gating for 3-dimensional PET of the thorax: feasibility and initial results *J. Nucl. Med.* **45** 214–9

Calabrese P, Dinh T P, Eberhard A, Bachy J P and Benchetrit G 1998 Effects of resistive loading on the pattern of breathing *Respiration Phys.* **113** 167–79

Chandarana H, Heacock L, Rakheja R, DeMello L R, Bonavita J, Block T K, Geppert C, Babb J S and Friedman K P 2013 Pulmonary nodules in patients with primary malignancy: comparison of hybrid PET/MR and PET/CT imaging *Radiology* **268** 874–81

Cheng C-C, Belsley G, Moore S, Preiswerk F, Wu P-H, Kijewski M, Campbell L, DiCarli M and Madore B 2018 Ultrasound-based sensors for motion correction of PET data. *Proc. Society of Nuclear Medicine and Molecular Imaging (Philadelphia, PA, USA)* p 8

Chi P C, Balter P, Luo D, Mohan R and Pan T 2006 Relation of external surface to internal tumor motion studied with cine CT *Med. Phys.* **33** 3116–23

Dasari P, Johnson K, Dey J, Lindsay C, Shazeeb M, Mukherjee J, Zheng S and King M 2014a MRI Investigation of the linkage between respiratory motion of the heart and markers on patient's abdomen and chest: implications for respiratory amplitude binning list-mode PET and spect studies *IEEE Trans. Nucl. Sci.* **61** 192–201

Dasari P K, Shazeeb M S, Konik A, Lindsay C, Mukherjee J M, Johnson K L and King M A 2014b Adaptation of the modified Bouc–Wen model to compensate for hysteresis in respiratory motion for the list-mode binning of cardiac SPECT and PET acquisitions: testing using MRI *Med. Phys.* **41** 112508

Dasari P K, Konik A, Pretorius P H, Johnson K L, Segars W P, Shazeeb M S and King M A 2017 Correction of hysteretic respiratory motion in SPECT myocardial perfusion imaging: simulation and patient studies *Med. Phys.* **44** 437–50

Dawood M, Lang N, Jiang X and Schafers K P 2006 Lung motion correction on respiratory gated 3D PET/CT images *IEEE Trans. Med. Imaging* **25** 476–85

Dawood M, Buther F, Lang N, Schober O and Schafers K P 2007 Respiratory gating in positron emission tomography: a quantitative comparison of different gating schemes *Med. Phys.* **34** 3067–76

Erdi Y E *et al* 2004 The CT motion quantitation of lung lesions and its impact on PET-measured SUVs *J. Nucl. Med.* **45** 1287–92

Fayad H, Pan T, Pradier O and Visvikis D 2012 Patient specific respiratory motion modeling using a 3D patient's external surface *Med. Phys.* **39** 3386–95

Günther M and Feinberg D A 2004 Ultrasound-guided MRI: preliminary results using a motion phantom *Magn. Reson. Med.* **52** 27–32

Hess M, Buther F and Schafers K P 2017 Data-driven methods for the determination of anterior-posterior motion in PET *IEEE Trans. Med. Imaging* **36** 422–32

Hope T A, Verdin E F, Bergsland E K, Ohliger M A, Corvera C U and Nakakura E K 2015 Correcting for respiratory motion in liver PET/MRI: preliminary evaluation of the utility of bellows and navigated hepatobiliary phase imaging *EJNMMI Phys.* **2** 21

Keller S H, Holm S, Hansen A E, Sattler B, Andersen F, Klausen T L, Hojgaard L, Kjaer A and Beyer T 2013 Image artifacts from MR-based attenuation correction in clinical, whole-body PET/MRI *MAGMA* **26** 173–81

Kesner A L, Schleyer P J, Buther F, Walter M A, Schafers K P and Koo P J 2014 On transcending the impasse of respiratory motion correction applications in routine clinical imaging—a consideration of a fully automated data driven motion control framework *EJNMMI Phys.* **1** 8

Koch N, Liu H H, Starkschall G, Jacobson M, Forster K, Liao Z, Komaki R and Stevens C W 2004 Evaluation of internal lung motion for respiratory-gated radiotherapy using MRI: I. Correlating internal lung motion with skin fiducial motion *Int. J. Radiat. Oncol., Biol., Phys.* **60** 1459–72

Kording F, Schoennagel B, Lund G, Ueberle F, Jung C, Adam G and Yamamura J 2015 Doppler ultrasound compared with electrocardiogram and pulse oximetry cardiac triggering: a pilot study *Magn. Reson. Med.* **74** 1257–65

Liu C, Alessio A M and Kinahan P E 2011 Respiratory motion correction for quantitative PET/CT using all detected events with internal-external motion correlation *Med. Phys.* **38** 2715–23

Lu W, Parikh P J, Hubenschmidt J P, Bradley J D and Low D A 2006 A comparison between amplitude sorting and phase-angle sorting using external respiratory measurement for 4D CT *Med. Phys.* **33** 2964–74

Madore B, Preiswerk F, Bredfeldt J S, Zong S and Cheng C C 2021 Ultrasound-based sensors to monitor physiological motion *Med. Phys.* **48** 3614–22

McClelland J R, Hawkes D J, Schaeffter T and King A P 2013 Respiratory motion models: a review *Med. Image Anal.* **17** 19–42

Nehmeh S A *et al* 2004 Four-dimensional (4D) PET/CT imaging of the thorax *Med. Phys.* **31** 3179–86

Nehmeh S A and Erdi Y E 2008 Respiratory motion in positron emission tomography/computed tomography: a review *Semin. Nucl. Med.* **38** 167–76

Nehmeh S A, Erdi Y E, Ling C C, Rosenzweig K E, Schoder H, Larson S M, Macapinlac H A, Squire O D and Humm J L 2002 Effect of respiratory gating on quantifying PET images of lung cancer *J. Nucl. Med.* **43** 876–81

O'Connor J M, Pretorius P H, Johnson K and King M A 2013 A method to synchronize signals from multiple patient monitoring devices through a single input channel for inclusion in list-mode acquisitions *Med. Phys.* **40** 122502

Osman M M, Cohade C, Nakamoto Y and Wahl R L 2003 Respiratory motion artifacts on PET emission images obtained using CT attenuation correction on PET-CT *Eur. J. Nucl. Med. Mol. Imaging* **30** 603–6

Petrusca L *et al* 2013 Hybrid ultrasound/magnetic resonance simultaneous acquisition and image fusion for motion monitoring in the upper abdomen *Investigative Radiol.* **48** 333–40

Pfanner F, Maier J, Allmendinger T, Flohr T and Kachelriess M 2013 Monitoring internal organ motion with continuous wave radar in CT *Med. Phys.* **40** 091915

Pichler B J, Wehrl H F, Kolb A and Judenhofer M S 2008 Positron emission tomography/magnetic resonance imaging: the next generation of multimodality imaging? *Semin. Nucl. Med.* **38** 199–208

Preiswerk F, Cheng C C, Luo J and Madore B 2018 Synthesizing dynamic MRI using long-term recurrent convolutional networks *9th Int. Conf. on Machine Learning in Medical Imaging*

Preiswerk F, Toews M, Cheng C C, Chiou J G, Mei C S, Schaefer L F, Hoge W S, Schwartz B M, Panych L P and Madore B 2017 Hybrid MRI-ultrasound acquisitions, and scannerless real-time imaging *Magn. Reson. Med.* **78** 897–908

Preiswerk F, Toews M, Hoge W S, Chiou J-Y, Panych L, Wells W III and Madore B 2015 Hybrid utrasound and MRI acquisitions for high-speed imaging of respiratory organ motion *Medical Image Computing and Computer-Assisted Intervention—MICCAI* ed N Navab *et al* (Berlin: Springer) pp 315–22

Raad R A, Friedman K P, Heacock L, Ponzo F, Melsaether A and Chandarana H 2016 Outcome of small lung nodules missed on hybrid PET/MRI in patients with primary malignancy *J. Magn. Reson. Imaging* **43** 504–11

Ren S, Jin X, Chan C, Jian Y, Mulnix T, Liu C and Carson R E 2017 Data-driven event-by-event respiratory motion correction using TOF PET list-mode centroid of distribution *Phys. Med. Biol.* **62** 4741–55

Riola-Parada C, Garcia-Canamaque L, Perez-Duenas V, Garcerant-Tafur M and Carreras-Delgado J L 2016 Simultaneous PET/MRI versus PET/CT in oncology. A systematic review *Rev. Esp. Med. Nucl. E Imagen Mol.* **35** 306–12

Ruan D, Fessler J A, Balter J M, Berbeco R I, Nishioka S and Shirato H 2008 Inference of hysteretic respiratory tumor motion from external surrogates: a state augmentation approach *Phys. Med. Biol.* **53** 2923–36

Sawicki L M, Grueneisen J, Buchbender C, Schaarschmidt B M, Gomez B, Ruhlmann V, Umutlu L, Antoch G and Heusch P 2016a Evaluation of the outcome of lung nodules missed on 18F-FDG PET/MRI compared with 18F-FDG PET/CT in patients with known malignancies *J. Nucl. Med.* **57** 15–20

Sawicki L M, Grueneisen J, Buchbender C, Schaarschmidt B M, Gomez B, Ruhlmann V, Wetter A, Umutlu L, Antoch G and Heusch P 2016b Comparative performance of 18F-FDG PET/MRI and 18F-FDG PET/CT in detection and characterization of pulmonary lesions in 121 oncologic patients *J. Nucl. Med.* **57** 582–6

Schleyer P J, O'Doherty M J and Marsden P K 2011 Extension of a data-driven gating technique to 3D, whole body PET studies *Phys. Med. Biol.* **56** 3953–65

Schleyer P J, Thielemans K and Marsden P K 2014 Extracting a respiratory signal from raw dynamic PET data that contain tracer kinetics *Phys. Med. Biol.* **59** 4345–56

Willey D, Bresticker J, Truong T-K, Song A, Madore B and Darnell 2020 Integrated RF/wireless coil and ultrasound-based sensors to enable wireless physiological motion monitoring in MRI *Proc. Int. Society of Magnetic Resonance in Medicine, (Virtual Meeting)*, p 1282

Zhang T, Keller H, O'Brien M J, Mackie T R and Paliwal B 2003 Application of the spirometer in respiratory gated radiotherapy *Med. Phys.* **30** 3165–71